applied sciences

MDPI

*Article*

# Enhanced Wear Resistance of Microstripe-Textured Water-Lubricated Materials Fabricated via Hot Embossing

**Zeyun Li [1,2], Weibin Wu [1,2,*], Xue Yang [1,2] and Xin Wang [1,2]**

[1] Institute of Noise and Vibration, Naval University of Engineering, Wuhan 430033, China; lizeyun@alumni.nudt.edu.cn (Z.L.); yang2014xue@163.com (X.Y.); yikaleide@whu.edu.cn (X.W.)
[2] Key Laboratory on Ship Vibration & Noise, Wuhan 430033, China
* Correspondence: wuweibin0910@163.com

**Abstract:** Water-lubricated material is the fundamental ingredient of a water-lubricated bearing (WLB), of which the friction and wear properties directly affect the working performance and service life of a WLB. We designed a micron-scale stripe texture and fabricated a negative microtexture mold by femtosecond laser etching. The microtextures were fabricated onto the surface of Thordon and polyurethane water-lubricated materials by a precision thermoforming machine. Tribological tests showed that the microstripe texture on water-lubricated materials had lower friction and wear properties than that on pristine surface materials. The results demonstrated that the presence of the microstripe texture effectively improved the friction and anti-wear properties of the water-lubricated materials. This study provides a new idea for the design and preparation of water-lubricated materials with good water-lubricating and anti-wear properties.

**Keywords:** water-lubricated material; surface microtexture; tribological properties; ultra-precision machining



**Citation:** Li, Z.; Wu, W.; Yang, X.; Wang, X. Enhanced Wear Resistance of Microstripe-Textured Water-Lubricated Materials Fabricated via Hot Embossing. *Appl. Sci.* **2024**, *14*, 4625. https://doi.org/10.3390/app14114625

Academic Editor: Mark J. Jackson

Received: 20 April 2024
Revised: 20 May 2024
Accepted: 20 May 2024
Published: 28 May 2024



## 1. Introduction

Water-lubricated bearings are important support devices for the propulsion shaft systems of underwater vehicles. Improving their lubrication conditions and load-bearing capacity are important measures to improve the safety and concealment of underwater vehicles [1–4]. In practice, water-lubricated bearings generally exist in dynamic pressure lubrication or mixed lubrication states [5,6]. However, at low speeds, under heavy loads and starting and stopping conditions, the formation of a hydrodynamic film between the bearing and the shaft will be difficult, causing some areas to be under a boundary lubrication state or even experience dry friction. This will lead to a rapid deterioration in interface lubrication, which in turn causes abnormal wear of the bearing lining [7,8]. Over the past two decades, the surface microtexture has been proven to be one of the effective technological tools in tribology for improving lubrication, increasing load capacity, and reducing friction and wear [9–14].

Ultra-precision machining technology is capable of achieving sub-micron-level shape accuracy and nanometer-level surface roughness precision, representing the highest level of manufacturing precision [15]. Ultra-precision machining technology can achieve the high-precision fabrication of functional surfaces with complex micro- and nanostructures [16]. Thanks to this, it is possible to customize micro- and nano-textures on the surface of water-lubricated bearings using ultra-precision machining technology to improve the tribological properties of water-lubricated materials [17,18].

In this study, a micron-scale stripe texture was designed, a mold with negative microstripe textures was processed by femtosecond laser etching, and the microtextures were fabricated onto the surfaces of two types of water-lubricated material (Thordon and polyurethane) by a precision thermoforming method. Tribological tests revealed that the microstripe-textured water-lubricated materials exhibit lower friction and less wear than

the original materials, and the results demonstrated that the presence of the microstripe texture effectively improves the friction and anti-wear properties of the water-lubricated materials. This paper provides a new idea for the design and fabrication of water-lubricated materials with superior water-lubricating and anti-wear properties.

## 2. Materials and Methods

### *2.1. Materials' Preparation*

Two kinds of water-lubricated materials, i.e., polyurethane (PU) and Thordon COMPAC water-lubricated material (Thordon Corporation, Burlington, ON, Canada, hereinafter referred to as "Thordon"), were used as substrates for embedding the microstripe texture. All materials were manufactured into a block shape (19.05 × 12.32 × 12.32 mm) by a small CNC milling machine (SX201683n, Guanglong CNC equipment Manufacturing Co., Ltd., Hefei, China). Before microtexture fabrication, the surfaces were carefully polished to a roughness of Ra1.6.

### *2.2. Manufacturing Method of Microtextured Surfaces*

The microstripe textures were embedded onto the surface of the water-lubricated materials with a hot-embossing method [19,20]. Figure 1 shows the precision of the hot-pressing machine utilized in this study. The right side of the machine is the program control console, and the left side is the processing station. The machine is equipped with an internal hydraulic station for the downward and upward movement of the cylinders and the maintenance of constant pressure. The precision hot-pressing machine is equipped with upper and lower heating plates for heating and pressurizing the mold.

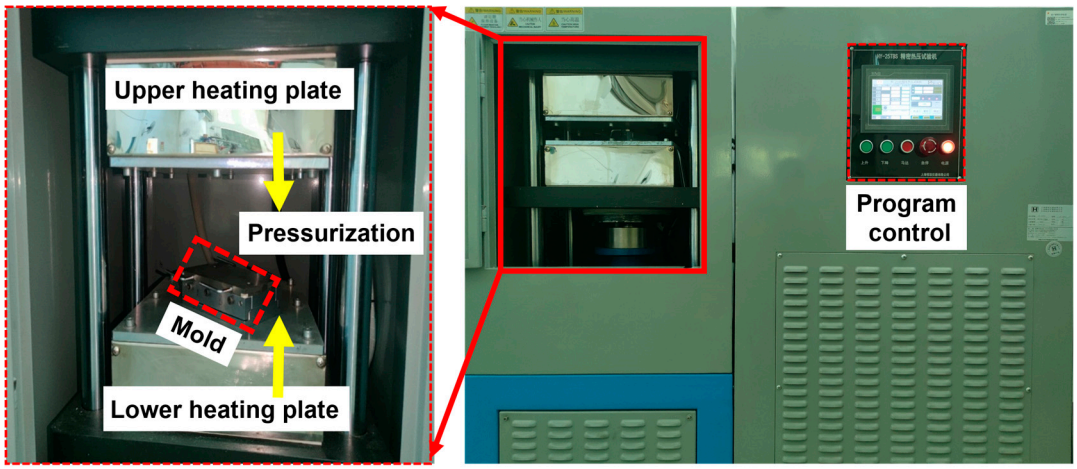


**Figure 1.** The precision hot-pressing machine applied in this study.

With the advantage of scanning along a pre-set path with extra-high precision, laser etching technology is often used to process material surfaces to fabricate textured structures at the microscale [21]. A steel mold with four tabs and corresponding concave containers was designed and fabricated, as shown in Figure 2a. The mold was made of Stavax ESR (ASSAB Pacific Pte. Ltd. SAN Centre Singapore) high-grade stainless steel with excellent corrosion resistance, high machinability, and dimensional stability in thermal treatment. A negative microstripe texture with a stripe spacing of 5 μm was designed and fabricated using femtosecond laser etching on the surfaces of the two upper tabs, while the other tabs were smooth surfaces. The corresponding 3D topographies of the surfaces are shown in Figure 2b. The results show that the negative microstripe texture was successfully manufactured on the objective mold surface by femtosecond laser etching technology.

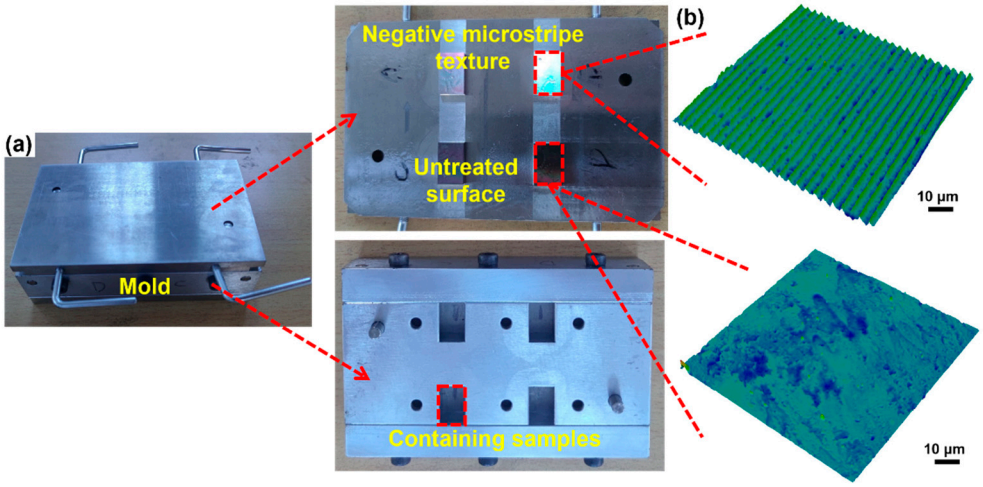


**Figure 2.** (**a**) The forming mold consists of two parts: a top plate with four convex terraces that were manufactured with a negative microstripe texture or finished as a pristine surface and a bottom substrate with four containers to place water-lubricated blocks. (**b**) The 3D topography images of the microstripe-textured and pristine surfaces. Periodic microstripe texture with intervals of 5 μm or pristine surface topography can be observed.

### *2.3. Tribological Tests*

A ring-block friction/wear tester (MRH-3G, Jinan Hengxu Tribological Testing Technology Co., Ltd., Jinan, China) was used to characterize the friction and wear properties of water-lubricated blocks. Ring rotation caused friction on the block (a normal load was applied from the top), which was recorded by the integrated force sensors. The wear scar of block surface was characterized by a laser microscope (Olympus LEXT OLS5100, Olympus Co., Ltd., Tokyo, Japan). Figure 3 shows a photo of the ring-block friction testing machine used for the friction and wear test. The ring was made of ZCuSn10Zn2, and the size (φ) was 49.22 × 13.05 mm. Each block (water-lubricated material) had a size of 19.05 × 12.32 × 12.32 mm.

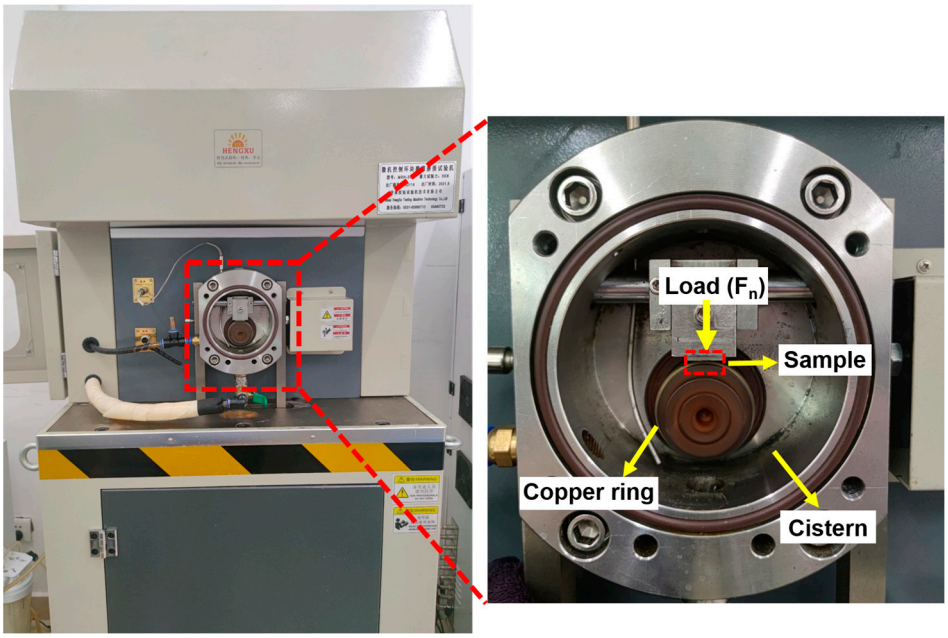


**Figure 3.** Picture of ring-block friction testing machine used for friction and wear testing. ($F_n$ is normal load.)

The coefficient of friction (COF) was determined as the ratio of the friction and normal forces. The specific wear rate was calculated according to [22]

$$W_s = V_s/F * 2\pi R * nt \quad (1)$$

where F, n, and t denote the normal load, ring rotary speed, and test time, respectively. R represents the radius of the corresponding copper ring. Vs is the wear volume of each specimen calculated according to the following equation [22]:

$$V_s = \left[ R^2 \frac{\pi}{180} \arcsin\frac{b}{2R} - \frac{b}{2}\sqrt{R^2 - \frac{b^2}{4}} \right] B \quad (2)$$

where b and B represent the widths of the abrasion marks and sample block. A friction/wear test for each material was repeated five times, and the average values together with the corresponding standard deviation were plotted for comparison.

To compare the friction and wear performance of the pristine surface and microstripe-textured specimens, a normal load of 50 N (the corresponding pressure is 0.2 MPa.) and rotary speed of 100 rpm (the corresponding linear velocity is 515.17 mm/s) were implemented. For comparison, tap water was used as the lubricant in the tribological tests under the same conditions. All the tests were conducted with water lubrication at a room temperature of 25 ± 2 °C and 35 ± 5% relative humidity for 120 min.

## 3. Results and Discussion

### *3.1. Fabrication of Microstripe Textures*

In order to solve the problem of abnormal wear on bearing linings at low speeds, heavy loads, and frequent start and stop conditions, and to improve the tribological performance and lubrication characteristics of the bearings, a regular microstripe texture was constructed on the surface of water-lubricated materials. The dimensions of the microtextures were the following: the spacing L between two adjacent stripes was 5 μm, and the depth H of the stripes was 0.5 μm. The direction of the stripe microtexture was aligned perpendicular to the direction of motion of the copper ring, as shown in Figure 4. The design of the microtexture was inspired by the microstructure of the epidermal scales of a lizard called sandfish (*Scincus scincus*). The dimensions of the microtexture (L and H) were based on the scale parameters of the lizard's epidermal scale microstructure.

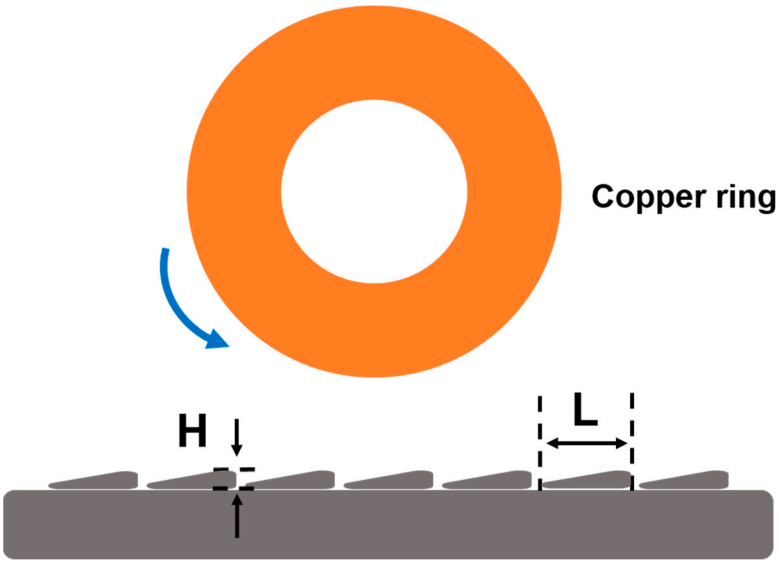


**Figure 4.** The schematic diagram of cross-section of microstripe texture.

The microstripe texture was fabricated onto the surface of the water-lubricated material by a hot-embossing method. The water-lubricated blocks were placed into the mold container, and the mold was then placed into the precision hot-pressing machine. Specific temperatures and pressures were applied to the mold according to the thermoplastic characteristics of the Thordon and polyurethane. After a certain forming time, Thordon and polyurethane samples featuring imprinted microstripe textures or pristine surfaces were obtained. All the samples were finally cleaned with acetone to remove residual material, dust, or other contaminants in preparation for tribological testing.

Table 1 summarizes the forming temperatures, pressures, and times for embossing the microstripe textures on the Thordon and polyurethane materials. The parameters for each material varied depending on their different thermoforming properties. Due to the poor fluidity of the thermoplastic polyurethane, it was not possible for the flow to spread evenly over a short period of time and it also could not overflow in time, resulting in the microstripe texture not being effectively embossed onto the surface of the material. Therefore, an extended pressing time for the polyurethane, as opposed to the Thordon material, allowed the melt to be fully fluidized and spread out so that the microtexture of the mold was fully embossed onto the surface of the material. The pictures of the Thordon and polyurethane blocks after hot embossing are shown in Figure 5a,d.

**Table 1.** Processing parameters for replicating microstripe textures on Thordon and PU surfaces.

| Material | Heating Temperature (°C) | Preheating Time (min) | Preset Pressure (kN) | Preloading Time (s) | Work Pressure (kN) | Hot Pressing Time (s) | Mold Opening Temperature (°C) |
|---|---|---|---|---|---|---|---|
| Thordon | 175 | 10 | 20 | 5 | 50 | 240 | 70 |
| PU | 170 | 10 | 20 | 50 | 40 | 2150 | 70 |

The topography of the Thordon and polyurethane samples was characterized by laser microscopy, and the results are shown in Figure 5b,e. Comparing the surface topographies of the samples, regular microstripes were successfully fabricated onto the surfaces of the Thordon and polyurethane materials by the hot-embossing technique. Figure 5c,f show the surface profile curves of the samples truncated by the red dashed lines in Figure 5b,e, respectively. It can be seen that the profile curves of the pristine surfaces show irregular bumps or pits, representing random micro-convex bodies and micro-pits that occur on the sample surfaces, whereas the profile curves passing through the microtextured surfaces reveal regular jagged shapes, indicating regular microstripes. The spacing between two neighboring stripes was about 5 μm, and the depth of the stripe monomer was about 0.5 μm. The results demonstrate that the microstripe texture was successfully fabricated on the surfaces of the Thordon and polyurethane materials by the hot-embossing technique.

Table 2 summarised the surface roughness (Sa) of Thordon and PU with pristine and microtextured surfaces. By comparing the roughness of the material surface, we found an interesting phenomenon that the roughness of the microtextured surface was lower than that of the pristine surface. This suggests that fabricating the microtextures on the surface of water-lubricated materials can reduce the microconvex bodies such as burrs on the surface and make the surface more regular, which leads to a lower roughness on the surface of the material. This is due to the fact that the pristine surface has a higher adhesion force than the microtextured surface (discussed in the following Section 3.3), which leads to part of the materials adhering to the mold during mold opening process without fully separating, resulting in some irregular burrs on the pristine surface.

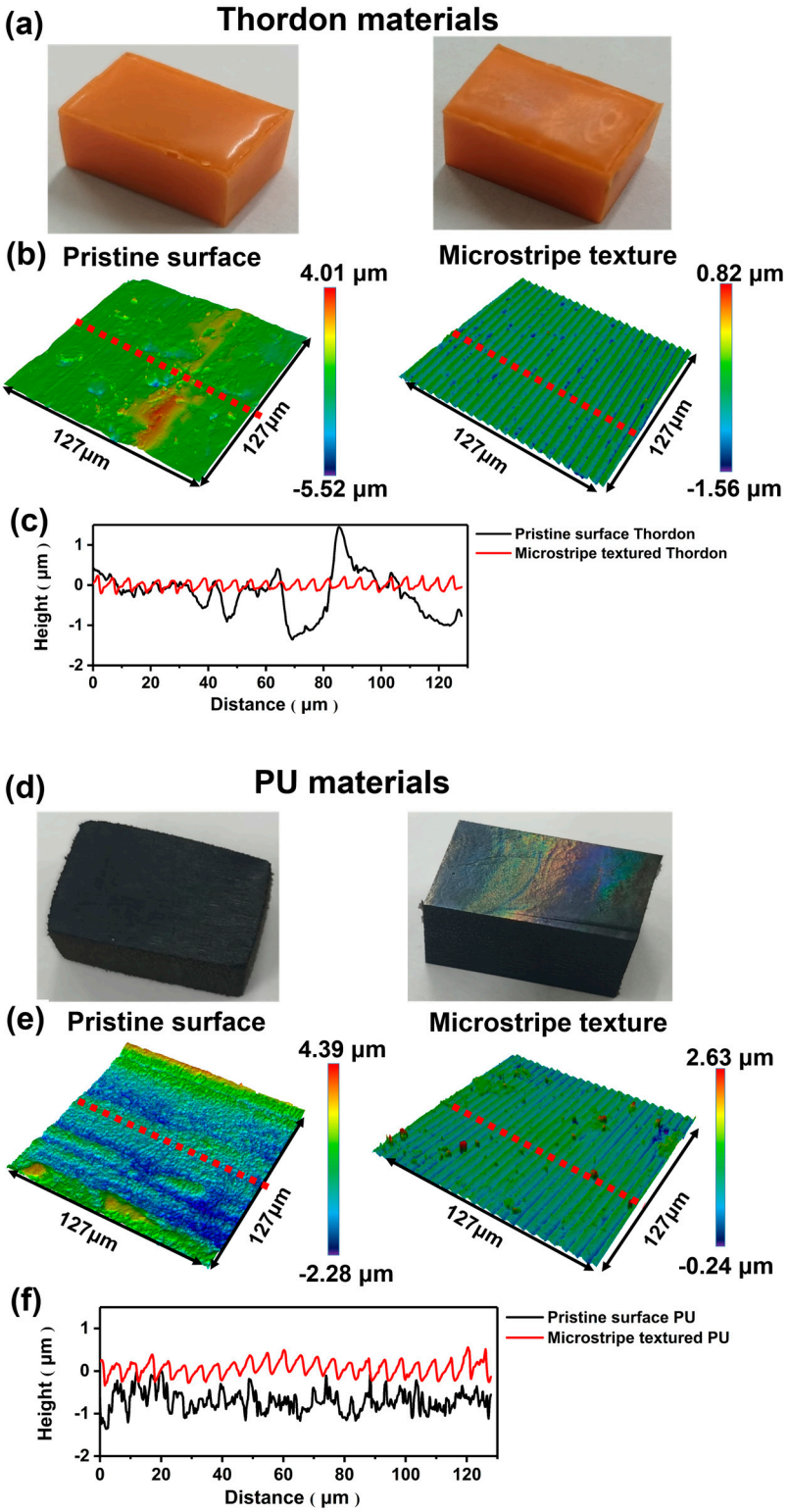


**Figure 5.** Picture and microscopic topography of the pristine surface and microstripe-textured water-lubricated blocks of (**a**–**c**) Thordon and (**d**–**f**) PU. (**a**,**d**) Photographs of each sample. (**b**,**e**) Corresponding morphology. (**c**,**f**) Height distribution profile along the red dashed line in the microscopic topography. The red dashed line is a random longitudinal tangent about the height of the topography in (**b**,**e**).

**Table 2.** Surface roughness of Thordon and PU with pristine and microtextured surfaces.

| Materials | Sa (μm) |
|---|---|
| Pristine surface Thordon | 0.084 |
| Microstripe-textured Thordon | 0.051 |
| Pristine surface PU | 0.203 |
| Microstripe-textured PU | 0.09 |

### *3.2. Effect of Microstripe Texture on the Water Contact Angle of Materials*

Water contact angles were measured for the pristine and microstripe-textured surfaces for the Thordon and polyurethane samples, as shown in Figure 6. For each sample, the mean values from five arbitrary locations and their corresponding standard deviations are shown. It can be seen that the water contact angle on the surface of the microstripe textured material increased slightly, by about 4°, compared to that of the water-lubricated material with a pristine surface. This result suggests that the microstripe texture contributes to the reduction in the surface energy of the water-lubricated material, thus potentially retarding the onset of adhesive wear.

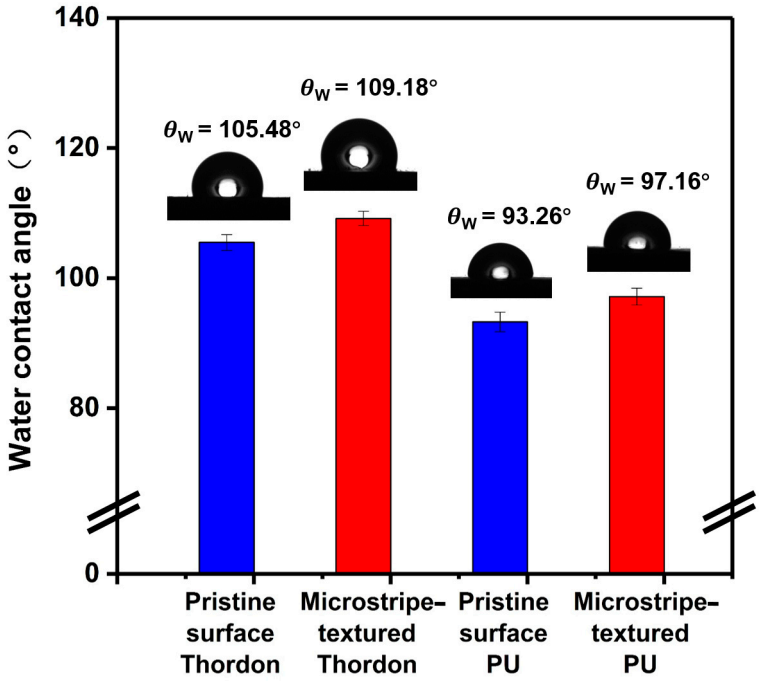


**Figure 6.** Water contact angle on Thordon and PU samples with pristine and microstripe-textured surfaces.

### *3.3. Influence of Microstripe Texture on the Adhesion of Materials*

To investigate the effect of the microstripe texture on the surface adhesion properties of the water-lubricated materials, the adhesion force between the samples and a silicon AFM tip was measured using atomic force microscopy (Dimension Edge, Bruker, Billerica, Germany). A sharp silicon tip of a commercial AFM cantilever was used to characterize the adhesion and friction properties of the sample surface in all the AFM experiment. A schematic image of the working principle of the typical AFM measurement is illustrated in Figure 7a. Atomic force microscopy allows the measurement of adhesion by recording force–distance curves [23]. Adhesion analysis of the sample surface was carried out in contact mode, i.e., the cantilever was fixed in the X and Y positions while bending in the Z direction. The force between the cantilever tip and the sample surface was calculated from the spring constant and the deflection sensitivity of the cantilever tip as it approached or detached from the sample surface. Figure 7a illustrates the theoretical force–distance

curve for the measurement of adhesion forces using AFM. The elastic constant of the cantilever was obtained from the manufacturer (0.4 N/m). All adhesion measurements for the experiment were carried out at a ramp frequency of 1 Hz with a velocity of 3.8 µm/s.

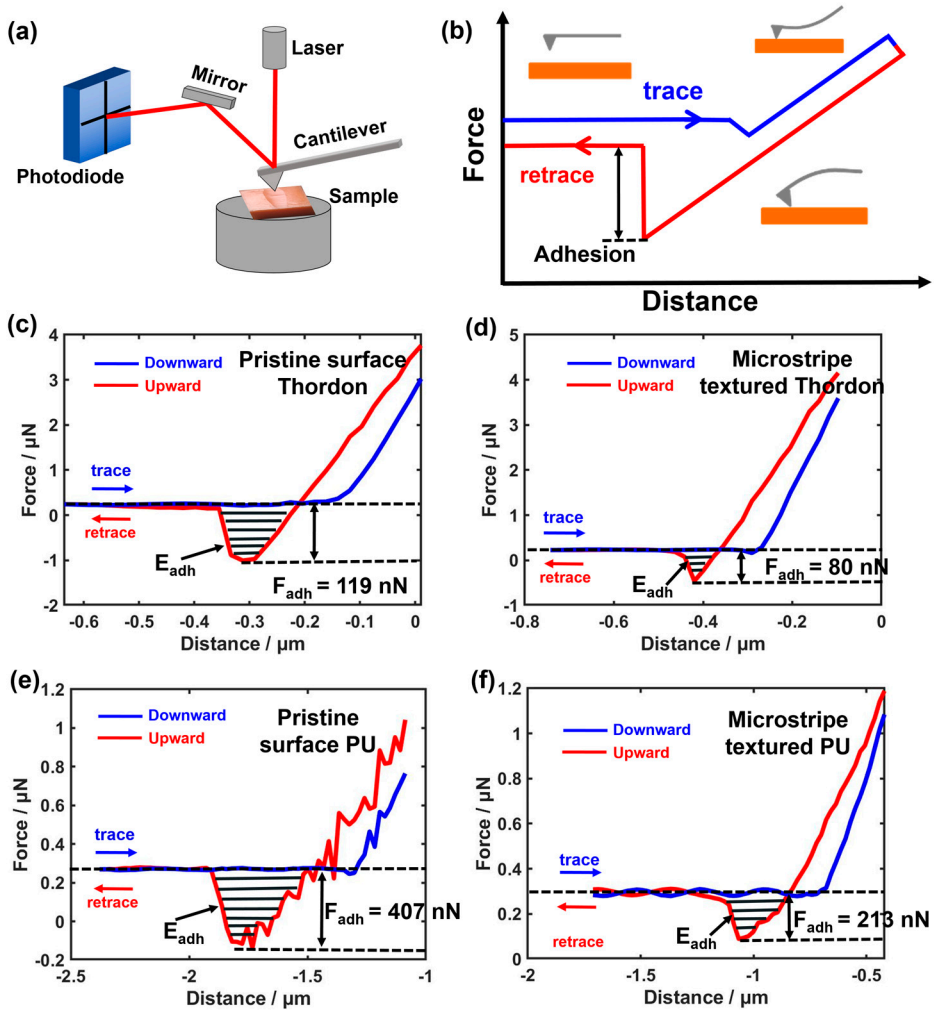


**Figure 7.** AFM-based adhesion measurement results. (**a**) Schematic detection principle of an AFM. A laser beam deflected at the backside of a cantilever detects its bending via a photodiode. The force between the cantilever tip and the sample surface was calculated from the spring constant and the deflection sensitivity of the cantilever tip as it approached or detached from the sample surface. (**b**) A theoretical force–distance curve shows an AFM tip measuring adhesion. The adhesion is evaluated as the maximum force required to retract the cantilever tip from the sample surface. (**c**–**f**) AFM-based adhesion measurements of Thordon and PU samples with pristine and microstripe-textured surfaces. The blue line and red line represent approach and retraction, respectively.

The silicon AFM tip moved towards the water-lubricated material sample and contacted the sample surface with a pre-defined load. Afterwards, the AFM cantilever was retracted until the silicon tips completely detached from the sample surface. Four typical force–distance curves recorded in this manner are shown in Figure 7c–f. The blue lines in the figure indicate trace motion, while red lines indicate retrace motion. The minimum value of the retrace force defines the adhesion force required to lift the AFM tip from the sample surface. The shaded area between the zero and retrace lines is defined as the adhesion energy required to disengage the probe from the sample surface [24]. Each specimen was tested at five arbitrary positions, and the adhesion force was measured five times at each point. The average of 25 adhesion tests was taken as the adhesion force of the sample.

Figure 7 clearly shows that the adhesion force of the Thordon with a microstripe texture on the surface was 80 nN, which is significantly lower than the adhesion force of 119 nN for the Thordon with a pristine surface, leading to a reduction of about 32.8%. In the case of polyurethane, the magnitude of adhesion force reduction was approximately 47.7%. For the adhesion energies, the adhesion work of the Thordon on the pristine surface was 166.8 fJ, and that of the Thordon with microstripe texture was 59.7 fJ, representing a reduction of about 64.2% in the adhesion work. The value for polyurethane was approximately 38.9%. The results show that embedding a microstripe texture on the surface of water-lubricated material helps to reduce the adhesion on the material surface, thereby attenuating the occurrence of adhesive wear.

### *3.4. Comparison of Tribological Properties between Pristine and Microtextured Surfaces*

Microscopic measurements recording friction vs. normal force curves on Thordon and polyurethane with pristine and microstripe-textured surfaces were recorded by AFM. The results are shown in Figure 8. The scanning size was set to 50 μm × 50 μm. For each measurement, a friction loop [25] was recorded for the AFM tip scanning in the forward and backward directions with a varying normal force. The averaged friction forces for both directions were calculated. For each sample, three different positions were analyzed, and the results were averaged into each single data point in Figure 8. Increasing the defined normal force $F_{load}$ and recording the frictional force $F_{fric}$, the friction coefficient $\mu$ can be calculated by linearly fitting the applied load and its corresponding friction data ($F_{fric} = F_{adh} + \mu \times F_{load}$).

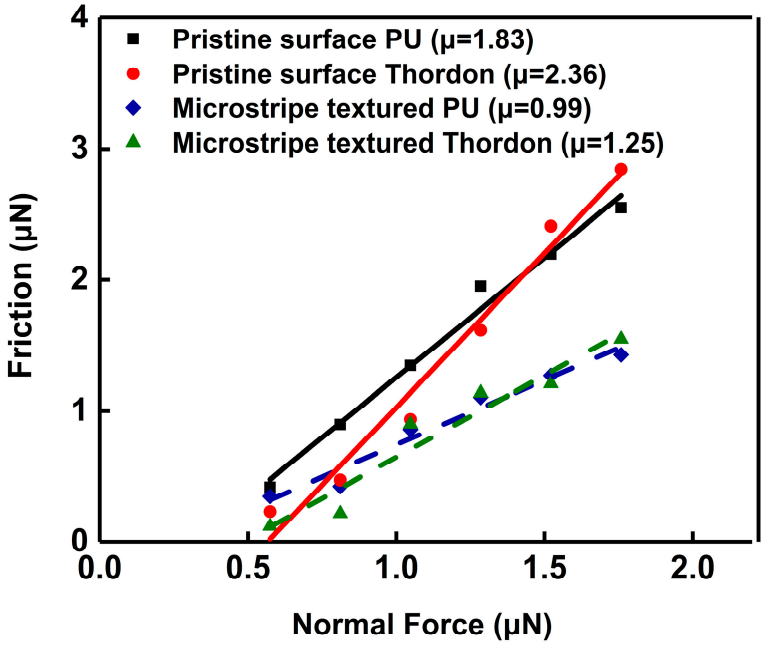


**Figure 8.** AFM-based friction measurement of Thordon and PU with pristine and microstripe-textured surfaces. The straight line in the figure was fitted to obtain the slope of the line, i.e., the friction coefficient μ.

As shown in Figure 8, the data show a nearly linear relationship between the normal loads and friction forces. The friction coefficient $\mu$ was calculated as the slope of this linear fit (provided in the legend) and was compared between the results for the pristine and microstripe-textured surfaces. For polyurethane, the friction coefficient of the pristine surface decreased from 1.83 to 0.99 with the introduction of a microstripe-textured structure, and this value decreased from 2.36 to 1.25 for the Thordon. This suggests that the presence of microstripe textures can effectively reduce the friction on water-lubricated materials.

Figure 9 shows the friction (Figure 9a), average coefficient of friction (COF), and specific wear rate (Figure 9b) of the above samples for the 2 h friction test conducted at a 50 N load, 100 r/min rotary speed, and water lubrication in the ring-on-block friction/wear test. As shown in Figure 9a, the friction of all Thordon samples was greater than that of the polyurethane samples. In addition, compared to Thordon, the friction trend of polyurethane was more stable over time, while the friction jitter amplitude of Thordon was larger, which was determined by the material's properties. Combined with the analysis of the surface morphology after abrasion, this is due to the fact that the abrasion mark on Thordon is deeper than that on polyurethane, by about 8–9 times. In particular, it is interesting to note that for the same material, surfaces with microstripe textures always exhibited lower friction than the pristine surfaces. This suggests that the microstripe texture contributed to the reduction in friction on the water-lubricated materials.

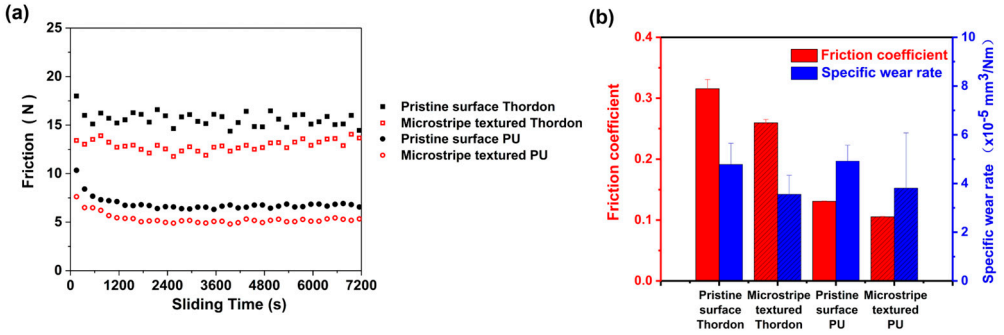


**Figure 9.** Comparison of friction and wear performance between pristine surfaces and microstripe-textured surfaces fabricated on Thordon and PU. (**a**) Friction forces recorded during a 120 min ring-block friction/wear experiment. Lower friction was observed on the microstripe-textured surface than on the pristine surface for each material. (**b**) Average COF and specific wear rate of all the tested specimens. The error bar in the figure represents the standard deviation of each dataset.

Figure 9b shows that the samples with microstripe-textured surfaces demonstrated a lower coefficient of friction and wear rate relative to the samples with pristine surfaces. The COFs of Thordon and PU with microstripe-textured surfaces were reduced by about 17.7% and 19.8%, respectively, compared to the pristine surfaces. In terms of wear performance, the wear rates of Thordon and PU with microstripe-textured surfaces were reduced by 27.3% and 25.5%, respectively, compared to those of the samples with pristine surfaces. The excellent tribological properties of microstripe-textured surfaces can be attributed to several factors. Firstly, the microtexture reduces the actual contact area and adhesion between the friction pairs, resulting in lower friction. In addition, the microtexture, with a depth of 0.5 μm between the stripes, helps to trap abrasive particles and can reduce the occurrence of abrasive wear. Finally, the uniformly arranged microstripe texture contributes to the rapid formation of a stable lubricating water film, which in turn improves the lubrication state between the friction pairs, thus reducing the friction and wear properties of the material.

A summary of the photographs, 3D topographies, and 2D profiles (perpendicular to microstrips, marked in red lines) of the Thordon and PU samples after the friction experiments is shown in Figure 10. The widths of the abrasion scar were about 8.5 mm and 6.4 mm, and the depths were about 234 μm and 165 μm for the Thordon samples with pristine and microstripe-textured surfaces, respectively. Microstripe-textured Thordon demonstrated a smaller abrasion width and depth than the pristine surface sample, where the width and depth of the wear scar were lower by 24.7% and 29.5%, respectively. The width and depth of the wear scar on the microstripe-textured PU reduced by approximately 5.7% and 17.4% compared to those of the pristine surface sample. The reason for this may be that the microstripe texture contributes to the formation of a stable lubricating water film, which provides a certain load-bearing capacity under dynamic pressure lubrication, reducing the load of the copper ring acting on the surface of the material. Thus, it can be

concluded that embedding microstripe textures can improve the tribological properties of water-lubricated materials, such as optimizing the formation of a lubricating water film, reducing adhesion, friction, and wear, thereby leading to a superior anti-wear performance compared to pristine surfaces.

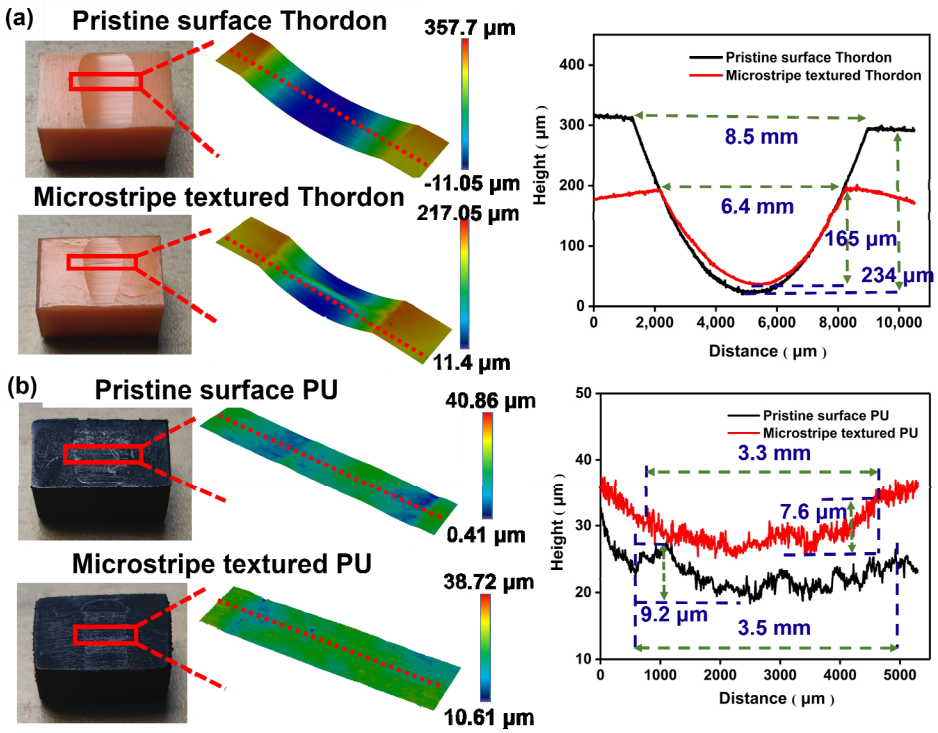


**Figure 10.** Topography characterization of wear marks on (**a**) pristine surface and microstripe-textured Thordon blocks, (**b**) pristine surface and microstripe-textured PU block. Photos and laser microscopic images of wear scar are shown in left and middle. Line section profiles along red dashed lines in the middle column are summarized in the right-side charts. Results for the pristine and microstripe-textured surface of the same material are plotted in the same chart for comparison.

## 4. Conclusions

In conclusion, we processed molds with negative microstripe textures using femtosecond laser etching and embedded microstripe textures onto the surfaces of Thordon and polyurethane materials using a precision hot-embossing method. The experimental results show that the microtextured surface demonstrates lower surface energy and lower adhesion than the pristine surface, which can reduce the generation of adhesive wear. The tribological test results reveal that the microstripe textures effectively reduce the friction on material surface by about 20% compared to that on the pristine surface samples, and significantly improving the anti-wear performance of the material, with the wear rate reduced by approximately 30%. The results indicate that the presence of a microstripe texture effectively improves the tribological properties of water-lubricated materials. This method provides a new idea for the development of water-lubricated materials with high reliability, high stability, and superior anti-wear performance.

**Author Contributions:** Conceptualization, W.W. and Z.L.; validation, W.W.; formal analysis, X.Y. and X.W., investigation, Z.L. and X.Y.; data curation, Z.L.; writing—original draft, Z.L. and W.W.; supervision, W.W., funding acquisition, X.W. All authors have read and agreed to the published version of the manuscript.

**Funding:** This work was financially supported by the National Natural Science Foundation of China (grant No. 52201390), the Natural Science Foundation of Hubei Province (grant No. 2022CFB866), as well as the foundation of the National Key Laboratory on Ship Vibration and Noise (JCKY2021207CI03,

JCKY2022207CI07), and the National Defense Project for Foundation En-hancement (2020-JCJQ-ZD-204-00).

**Institutional Review Board Statement:** Not applicable.

**Informed Consent Statement:** Not applicable.

**Data Availability Statement:** The raw data supporting the conclusions of this article will be made available by the authors on request.

**Conflicts of Interest:** The authors declare no conflicts of interest.

## References

1. Dong, C.; Yuan, C.; Bai, X.; Yan, X.; Peng, Z. Study on wear behaviour and wear model of nitrile butadiene rubber under water lubricated conditions. *RSC Adv.* **2014**, *4*, 19034–19042. [CrossRef]
2. Wodtke, M.; Litwin, W. Water-lubricated stern tube bearing—Experimental and theoretical investigations of thermal effects. *Tribol. Int.* **2021**, *153*, 106608. [CrossRef]
3. Qin, H.-L.; Zhou, X.-C.; Zhao, X.-Z.; Xing, J.-T.; Yan, Z.-M. A new rubber/UHMWPE alloy for water-lubricated stern bearings. *Wear* **2015**, *328–329*, 257–261. [CrossRef]
4. Tang, D.; Xiao, K.; Xiang, G.; Cai, J.; Fillon, M.; Wang, D.; Su, Z. On the nonlinear time-varying mixed lubrication for coupled spiral microgroove water-lubricated bearings with mass conservation cavitation. *Tribol. Int.* **2024**, *193*, 109381. [CrossRef]
5. Han, H.S.; Lee, K.H. Experimental verification of the mechanism on stick-slip nonlinear friction induced vibration and its evaluation method in water-lubricated stern tube bearing. *Ocean. Eng.* **2019**, *182*, 147–161. [CrossRef]
6. Xie, Z.; Zhu, W. Theoretical and experimental exploration on the micro asperity contact load ratios and lubrication regimes transition for water-lubricated stern tube bearing. *Tribol. Int.* **2021**, *164*, 107105. [CrossRef]
7. Wu, W.; Li, S.; Yang, X.; Shuai, C.; Li, Z.; Wang, X. Improvement of the Static and Dynamic Characteristics of Water-Lubricated Bearings With Integrated Halbach Magnet Arrays. *Tribol. Trans.* **2023**, *66*, 302–315. [CrossRef]
8. Litwin, W. Experimental research on water lubricated three layer sliding bearing with lubrication grooves in the upper part of the bush and its comparison with a rubber bearing. *Tribol. Int.* **2015**, *82*, 153–161. [CrossRef]
9. Naduvinamani, N.B.; Fathima, S.T.; Jamal, S. Effect of roughness on hydromagnetic squeeze films between porous rectangular plates. *Tribol. Int.* **2010**, *43*, 2145–2151. [CrossRef]
10. Joshi, G.S.; Putignano, C.; Gaudiuso, C.; Stark, T.; Kiedrowski, T.; Ancona, A.; Carbone, G. Effects of the micro surface texturing in lubricated non-conformal point contacts. *Tribol. Int.* **2018**, *127*, 296–301. [CrossRef]
11. Hu, J.; Xu, H. Friction and wear behavior analysis of the stainless steel surface fabricated by laser texturing underwater. *Tribol. Int.* **2016**, *102*, 371–377. [CrossRef]
12. Dan, L.; Xuefeng, Y.; Chongyang, L.; Jian, C.; Shouren, W.; Yanjun, W. Tribological characteristics of a cemented carbide friction surface with chevron pattern micro-texture based on different texture density. *Tribol. Int.* **2020**, *142*, 106016. [CrossRef]
13. Wang, W.; He, Y.; Zhao, J.; Li, Y.; Luo, J. Numerical optimization of the groove texture bottom profile for thrust bearings. *Tribol. Int.* **2017**, *109*, 69–77. [CrossRef]
14. Pei, S.; Xu, H.; Yun, M.; Shi, F.; Hong, J. Effects of surface texture on the lubrication performance of the floating ring bearing. *Tribol. Int.* **2016**, *102*, 143–153. [CrossRef]
15. Li, R.; Du, X.; Zhang, Z. *Ultra-Precision Free-Form Surface Optical Design, Processing and Measurement Technology*; Machinery Industry Press: Beijing, China, 2015; p. 265. (In Chinese)
16. Kong, L.; Cheung, C. Design, fabrication and measurement of ultra-precision micro-structured freeform surfaces. *Comput. Ind. Eng.* **2011**, *61*, 216–225. [CrossRef]
17. Wang, L.; Zhao, X.; Guo, S.; Wang, M. Tribological properties of surface microtexture friction pairs under different lubrication conditions. *Adv. Mech. Eng.* **2019**, *11*, 1687814019881569. [CrossRef]
18. Wang, R.J.; Fu, B.Y.; Ma, L.; Yuan, T. Study on turbine vanes TBCs automatic spraying technology. *Therm. Spray. Technol.* **2015**, *7*, 1–5. (In Chinese)
19. Schroers, J.; Pham, Q.; Desai, A. Thermoplastic Forming of Bulk Metallic Glass—A Technology for MEMS and Microstructure Fabrication. *J. Microelectromechanical Syst.* **2007**, *16*, 240–247. [CrossRef]
20. Worgull, M. *Hot Embossing: Theory and Technology of Microreplication (Micro and Nano Technologies)*; Elsevier Ltd.: Oxford, UK, 2009; p. 368.
21. Jin, X.; Zheng, Y.; Zhang, Y.; Chen, Z.; Duan, X.; Fu, H.; Ji, J.; Yang, Z.; Hua, X.; Fu, Y. Hierarchical microtextures generated by pulsed-laser manufacturing for surface geometry modulation. *J. Manuf. Process.* **2023**, *97*, 148–158. [CrossRef]
22. Qu, C.; Wang, T.; Wang, Q.; Chen, S. A novel ternary interpenetrating polymer networks based on NBR/PU/EP with outstanding damping and tribological properties for water-lubricated bearings. *Tribol. Int.* **2022**, *167*, 107249. [CrossRef]
23. Leite, F.L.; Bueno, C.C.; Da Róz, A.L.; Ziemath, E.C.; Oliveira, O.N., Jr. Theoretical models for surface forces and adhesion and their measurement using atomic force microscopy. *Int. J. Mol. Sci.* **2012**, *13*, 12773–12856. [CrossRef] [PubMed]

24. Lutz, C.; Ma, Z.; Thelen, R.; Syurik, J.; Il'in, O.; Ageev, O.; Jouanne, P.; Hölscher, H. Analysis of Carbon Nanotube Arrays for Their Potential Use as Adhesives Under Harsh Conditions as in Space Technology. *Tribol. Lett.* **2019**, *67*, 10. [CrossRef]
25. Schwarz, U.D.; Koster, P.; Wiesendanger, R. Quantitative analysis of lateral force microscopy experiments. *Rev. Sci. Instrum.* **1996**, *67*, 2560–2567. [CrossRef]